School of Mathematical
and Physical Sciences

University of Reading

Department of Mathematics and Statistics

Preprint MPS-2012-11

31 May 2012

Superfast non-linear diffusion in porous media: new regimes, universal model and power laws

by

A.V. Lukyanov, M.M. Sushchikh, M.J. Baines and T.G. Theofanous

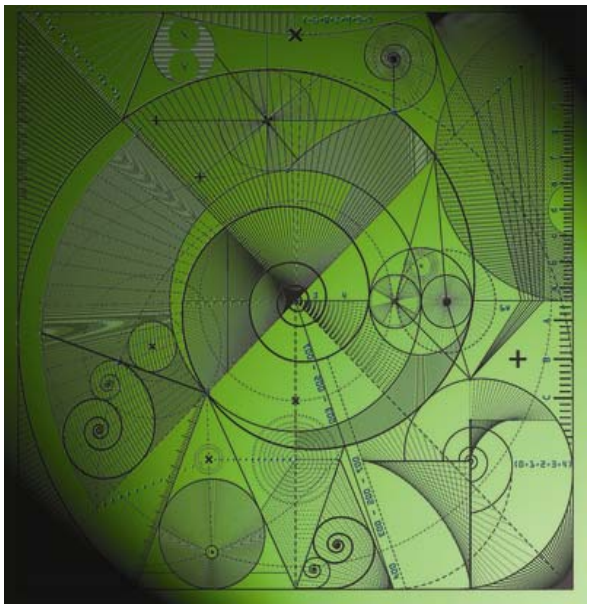

Superfast non-linear diffusion in porous media: new regimes, universal model and power laws.

A.V. Lukyanov[1], M.M. Sushchikh[2], M.J. Baines[1], T.G. Theofanous[2]

Department of Mathematics and Statistics, University of Reading, Reading RG6 6AX, U.K.[1]

Center for Risk Studies and Safety, University of California at Santa Barbara, Santa Barbara, CA, USA.[2]

Abstract

The migration of liquids driven by capillary forces in passage networks of porous media, such as sand, has been commonly considered at saturation levels relevant to pore dimensions. In this letter we reveal a very-low-saturation regime where the relevant length scales of the transport mechanics are defined by the grain roughness and by the capillary bridges at the contact points between grains. We demonstrate theoretically and support experimentally that this migration (or spreading) is a complex interplay between capillary pressure, as defined by the grain roughness and revealed by the bridges, and viscous losses of a microscopic, film-type, creeping flow taking place within the roughness. Incorporating properties of the liquid bridges as reservoirs, namely their pressure-volume dependence, yields the net macroscopic result which is a rather special case of diffusion, so far identified only in certain regimes of plasma physics, namely the superfast non-linear diffusion process. We propose a simple, but universal, model of this phenomenon and compare predictions with our experiments.

Non-volatile (persistent) liquids can spread significantly in porous substrates and cover large areas over long periods of time before they can be removed by evaporation. For example we found in experiments that a $6\,\mu$L drop of Tris(2-ethylhexyl) Phosphate (TEHP), deposited on a bed of ordinary sand, covered a volume of $\sim 6\,$mL in fifteen days; which with a bed porosity of $\sim 30\%$, suggests an equivalent saturation level of $s \sim 0.3\%$. The equilibrium vapor pressure of TEHP at room temperature is $P_s \simeq 10^{-5}\,$Pa, and for saturation s we use the common definition of volume occupied by liquid divided by the volume of accessible pore space. If the sand grains (average diameter of $\sim 250\,\mu$m) were round and smooth, specific surface area of $0.01\text{m}^2/\text{g}$, this saturation level translates to an average "film" thickness of $\sim 100 - 200$ nm, clearly a quantity that could be accommodated within the roughness of the sand particles. But what happens before such low levels are reached, how quickly may this happen, how far may this spreading process go, and in general how different is this regime in comparison to the well-studied process of penetration at saturation levels relevant to the pore length scales? To answer those questions we propose a macroscopic model based on microscopic principles describing transport at such low levels of saturation and compare results with experiments conducted specifically for this purpose.

To understand the distinctive features of this low-saturation regime we first consider the morphology of the liquid domains accommodated in a porous matrix consisting of spherical beads. This case has been investigated in the context of the mechanical properties of wet granular materials [1-3]. The experiments have been conducted with spherical glass particles of radii ranging from $R_0 = 140\,\mu$m to $R_0 = 600\,\mu$m agitated with water and allowed to settle to equilibrium. It has been found that, depending on the saturation level, the liquid domains may exhibit different topological features: (a) at the low end of saturations, $s_{min} < s < 7 - 8\%$, the liquid takes on predominantly the form of isolated pendular rings (or liquid bridges) formed between the spherical particles at the points of contact, (b) at higher saturations, $8\% < s <\simeq 24\%$, these bridges may coalesce into more complex structures like trimers, pentamers and heptamers, and (c) with further increases in saturation even larger clusters are found, untill finally at $s \approx 33\%$ the larger cluster comprises about 90% of the liquid volume in the porous matrix. The minimal value of the saturation at the onset of bridge formation (this also corresponds to the level at which the system loses its cohesive property) was found to be about $s_{min} \simeq 0.2\%$, [3].

Therefore it may be anticipated that in a more general case of natural systems, where a wetting liquid spreads in a matrix of roundish particles with rough surfaces, a similar trend with saturation levels applies; namely, two

principal regimes of spreading in particulate porous media: (a) a low-saturation regime, which is our present focus, in the range $s_{min} < s < s_{max}$, where s_{max} is a saturation level at which the liquid loses connectivity at the pore scale and, if the particles are impermeable, the transport may only occur within the roughness on the surfaces of the constituent particles, and (b) a high-saturation regime, in the range $s > s_{max}$, where the liquid domain is almost continuous everywhere, and the penetration process has a character of multiphase flow commonly studied in soil sciences [4]. (In the water-glass system $s_{max} \simeq 24\%$, and in our system we have found s_{max} as low as 20% using Micro X-ray Computer Tomography (MicroXCT) imaging, Fig. 1.) The relevant length scales are those of the roughness and the pores respectively, and gravity may be significant in the latter case only.

In accordance with the above, the saturation should actually be split into two contributions, $s = s_p + s_r$, where s_p corresponds to the liquid within the bridges and s_r to the liquid in the film contained within the surface roughness. As such, the process of migration of liquids in particulate porous media actually is an interplay between those two components, which clearly, in terms of the local capillary pressure must be in quasi-equilibrium. We show below that this can be expressed in the general form of Darcy's law [4], where the bridges are quantified so as to provide the average capillary pressure, while the film within the surface roughness controls the permeability. That is, the dynamics of continuous distributions of macroscopic (locally-averaged quantities) pressure p, velocity $\mathbf{v}$, and saturation s, relating liquid flux density $\mathbf{q} = \phi s \mathbf{v}$ to the pressure gradient will be expressed by:

$$\mathbf{q} = -\frac{k(s)}{\mu}\nabla p, \tag{1}$$

while for the equation of continuity we have:

$$\frac{\partial \phi\, s}{\partial t} + \nabla(\phi\, s\mathbf{v}) = 0 \tag{2}$$

where μ is viscosity of the liquid, and $k(s)$ and ϕ are the permeability and porosity of the porous network respectively.

For any macroscopic elementary volume in the porous matrix, one can relate the average pressure with the average amount of liquid contained in the capillary bridges, and thus with the saturation s_p. In the case of identical spheres (though not only) a relationship between the volume of the bridge and the mean curvature of the free surface of the bridge, and thus the pressure in the liquid, is available in an analytical although rather complex form [5]. In the case of two identical spheres in contact, for near-complete wetting systems, we have found that one can approximate (with maximum error less than 1%) normalised mean curvature HR_0 to normalised volume $V_p R_0^{-3}$ dependence derived in [5] by:

$$HR_0 = C_0 - C_1(V_p R_0^{-3})^{\gamma} \tag{3}$$

with $\gamma = -0.516 \pm 0.001$, which is consistent with the estimates obtained in [3] on p.229, and $C_1 = 1.3 \pm 0.002$, $C_0 = 3.7 \pm 0.01$. The negative value of $\gamma \approx -0.5$ is crucial in what follows.

Now, with the help of (3) the saturation s can be linked with the capillary pressure $p = 2\sigma H$ in the liquid bridges. Indeed, in a system of equal-size particles $s_p = \alpha_p^{-1} V_p R_0^{-3}$, $\alpha_p = \frac{4\pi}{3N_c}\frac{\phi}{1-\phi}$, N_c being the particle (liquid bridge) coordination number. Our experimental observations using MicroXCT reveal that for the sands used in our experiments N_c lies between 7 and 8. So, $s = \alpha_p^{-1} V_p R_0^{-3} + s_r$ and

$$p(s) = \frac{2\sigma}{R_0}\left\{C_0 - C_1\, \alpha_p^{\gamma}(s - s_r)^{\gamma}\right\}. \tag{4}$$

On the other hand, since the liquid flux in the low saturation regime occurs over the surface elements of the grains and through the bridges, the coefficient of permeability is defined by the topology of the surface roughness. It has been established previously, in the case of capillary flows over surfaces carved with various kinds of grooves

[6], and in a general case of quasi-static distribution of wetting liquids on rough surfaces [7], that the liquid completely fills the grooves (and here we assume that those results are applicable to our system too), so that $k \approx k_0 = const$ and $s_r \approx s_r^0 = const \approx \frac{1-\phi}{\phi}\frac{3\Delta R_0}{2R_0}$, where we have associated the size of the groove h_0 with the characteristic length scale of the surface roughness, ΔR_0. Moreover, in [6] it was found that the flow field obeys a local Darcy's law, $\mathbf{u} = -\frac{\kappa}{\mu}\nabla\psi$, where $\mathbf{u}$ is the velocity averaged over the groove length scale, ψ is the local liquid pressure, and κ is a local permeability. The latter is in general a function of geometric properties of the groove and the contact angle θ. For our case here $\theta \approx 0$ and κ is roughly proportional to the surface area of the groove cross-section $\kappa \approx \frac{\Delta R_0^2}{32\pi}$. If we now apply intrinsic liquid phase averaging, $< ... >^l = V_l^{-1}\int_{V_l} ... dV$, over the liquid volume V_l contained within the averaging volume V to the local Darcy's law, and make use of the spatial averaging theorem [8], we find

$$< \mathbf{u} >^l = -\frac{\kappa}{\mu}\nabla < \psi >^l = -\frac{\kappa}{\mu}\nabla p.$$

Now we consider a macroscopic surface element of area S and reduce the above equation to the area of entrances and exits for the liquid phase S_e through that surface element S, to obtain the liquid flux in (1)

$$\mathbf{q} = -\frac{\kappa}{\mu}\frac{S_e}{S}\nabla p.$$

The coefficient of permeability in (1) is thus obtained as $k_0 = \kappa\frac{S_e}{S}$, which may be given by $k_0 \approx 3\,(1-\phi)\frac{\Delta R_0^3}{32\pi R_0}$, since $\frac{S_e}{S} \approx 3(1-\phi)\frac{\Delta R_0}{R_0}$. More accurate estimation of the permeability and the film content as a function of saturation would need more detailed analysis of the flows over rough, and curved surfaces.

Now, using (4) one can cast (1) and (2) into a single non-linear diffusion equation,

$$\frac{\partial s}{\partial t} = D_0\nabla\left(\frac{\nabla s}{(s-s_r^0)^{1-\gamma}}\right) \quad \text{with} \quad D_0 = \frac{2\sigma}{R_0}\frac{k_0}{\mu}\frac{C_1|\gamma|\alpha_p^\gamma}{\phi}, \tag{5}$$

which is complemented with the boundary condition $s = s_F > s_r^0$ at the front moving with the velocity

$$\mathbf{v} = -D_0\frac{\nabla s}{s_F(s_F - s_r^0)^{1-\gamma}}.$$

Changing to new non-dimensional variables $\tilde{s} = (s - s_r^0)/s_{max}$, $\tilde{\mathbf{x}} = \mathbf{x}/L$ and $\tilde{t} = t/t_0$ with $t_0 = L^2 s_{max}^{1-\gamma}/D_0$, s_{max} and L being the maximum value of saturation and characteristic length scale at $t = 0$ respectively, we finally have

$$\frac{\partial\tilde{s}}{\partial\tilde{t}} = \nabla\left(\frac{\nabla\tilde{s}}{\tilde{s}^{1-\gamma}}\right). \tag{6}$$

In our case considered here $\gamma < 0$, which suggests that equation (6) belongs to the class of superfast non-linear diffusion equations found previously in a few applications in plasma physics [9]. The principal difference in the behaviour of solutions between the known porous-medium class of equations (PME) ($\gamma > 1$) and the superfast diffusion equation (SFDE) ($\gamma < 0$) is in the motion of the front and in the absence of self-similarity solutions to (5) in general [9]. In the case $\gamma > 1$, the small values of $\tilde{s} \approx 0$ at the front lead to the so called stagnation, for which $\tilde{v} \approx 0$ and waiting times occur before the front effectively starts moving [10]. This is clearly not the case in SFDE problems where, on the contrary, the front speed increases when the boundary value of $\tilde{s}$ decreases, though this may be moderated by the gradient of s. The absence of self-similarity solutions, on the other hand, leads to dependence of wet-volume propagation law on the initial conditions to (5). In particular, this manifests itself as different exponents q of the wet-volume-to-time power law $V(t) \sim t^q$ found in our experiments with different initial distributions, see some examples later in the text.

Now, we use this SFD model to address the rates of spreading at the special, low-saturation regime found in our experiments. As the test liquid we choose persistent TEHP obtained from Sigma-Aldrich [CAS 78-42-2] and as

the granular medium we use Standard Ottawa Sand (EMD Chemicals, Inc., p/n SX0075); it has an average grain size of 250 μm, porosity of 30% and surface roughness in the range $0.25 < \Delta R_0 < 3\,\mu$m [11]. The TEHP liquid has coefficient of surface tension $\sigma = 29$ mN/m, measured in our laboratory at $25^\circ C$ and viscosity $\mu \simeq 15\,$mPa $\cdot$ s at $20\,^\circ C$ [12]. The contact angles of TEHP measured from the image of a drop placed on either a sufficiently smooth or a rough flat glass surface were found to be close to $\theta_1^s \approx 10^\circ$ and $\theta_1^r \approx 0^\circ$ respectively, so that this choice of materials guaranties both effective capillary spreading and persistence.

The experiments were carried out by depositing imperceptibly a few microliter drops on naturally-packed sand beds, and following the evolution of the wet spot by time-lapse photography aided by UV-excited fluorescence using soluble Couymarin dye at concentration of 1% (w/w); the liquid properties remain unaffected. Experiments were run both in a full and a half-symmetry geometry modes; the latter made possible by a transparent, lyophobic wall (Teflon-coated glass) that allows optical access from the side (Fig. 2). The arrangement was left undisturbed for the duration of the tests, extending out to more than 10 days, and photographs were taken by two 10.7 MP computer-controlled digital cameras equipped with macrolenses and focused to resolve individual grains (Fig. 2). The lenses were fitted with longpass glass coloured filters to cut off scattered excitation light, such that no significant background signal could be detected in the absence of the dye in the range of exposures used in the experiments. Moreover, we have taken images at different values of the exposure to ensure confident capture of the wetted front position and have performed several multiply repeated series of experiments with different initial volume of the droplets at the full and half-symmetry geometries. In this way we found directly that, after some short initial transition period (sensitive to the details of the initial deposition), the shape of the wetted portion of sand is close to a hemisphere, Fig. 2, so that an equivalent wet volume and an average saturation can be accurately calculated from the measured radius of the wet area.

The results of two representative tests, involving two side-by-side 2.8 μL drops, at the full symmetry geometry are summarized in Fig. 3. The figure shows two main transition points that correspond to the start and the ending of the SFD regime and the limit saturation s_{lim} when the spreading stops. The corresponding saturations are found to be $s \simeq 20\%$, $s \simeq 1\%$ and $s_{lim} \simeq 0.55\%$, wet-volume follows a power law $V(t) \sim t^q$ with the exponent $q = 0.75$. In Figure 4, we show the SFD regime portion of the transient for 5 spots all created with 6 μL drops. One of these was at the full symmetry mode and two at the half-symmetry mode (two each, one depicting the volume based on the top surface of the bed and the other based on the side view). All 5 transients are well represented by the time-law found in Fig. 3 with $q = 0.65$, which starts at $s \simeq 10\%$. The spreading ends in all cases close to $s_{lim} \simeq 0.36\%$. One can notice a remarkable agreement in the value of q between the results obtained in the half and the full symmetry modes. Similar tests with Tricresyl Phosphate (TCP), another persistent liquid ($\sigma = 42.5$ mN/m, $\mu \simeq 20\,$mPa $\cdot$ s, $\theta_1^s \approx 30^\circ$, $\theta_1^r \approx 20^\circ$), have shown a very analogous behaviour and $q = 0.78$. As noted already, the limit saturation level corresponds to a uniform film of $100 - 200\,$nm suggesting that at the limit saturation of $s_{lim} \sim 0.3 - 0.6\%$ the film may lose connectivity at the bridges, which is consistent with what is known about the structural integrity of sands [2,3].

To compare the spreading law found in the experiments with what is predicted by our SFD model, we solve problem (5) numerically assuming spherical symmetry. The problem has three parameters D_0, s_F and s_r^0 and unknown initial condition taken in the form $s(r,0) = s_F + (s_C - s_F)\cos(\pi r/2)^\lambda$ on $r \in [0,1]$ parameterized by $2 < \lambda < 4$. In the simulations, we start at $s \simeq 10\%$ (the onset of the SFD regime in the case shown in Fig. 4) and define s_C from the experimental values. Parameter $s_F = 0.36\%$ has been obtained from the limit saturation s_{lim} observed in the experiments, which translates into $\Delta R_0 \simeq 120\,$nm. Since the coefficient of diffusion D_0 has no effect on the power law and only rescales time, we have determined $s_r^0 = 0.88\,s_F$ by matching the power law exponent q. Finally, the coefficient of diffusion $D_0 = 1.2 \times 10^{-14}\,\mathrm{m}^2/\mathrm{s}$ has been found by matching the whole volume-to-time dependence, while λ, used for fine tuning only, was set to $\lambda = 3.5$. This value of the diffusion coefficient corresponds to $\Delta R_0 \approx 160\,$nm at $N_c = 8$. The results of simulations are shown in Fig. 4.

In conclusion, we have found experimentally the spreading law at very low saturations in granular porous media. This regime initiates at liquid saturations $s \simeq 20\%$, manifests itself as a power law and ends at $s \simeq 1\%$. The spreading stops at $s_{lim} \simeq 0.3 - 0.6\%$, which is close to the level corresponding to the loss of structural cohesion. We have shown by a comparison of experimental results with numerical solutions to our SFD model that this spreading regime translates into a superfast non-linear diffusion process previously found only in certain problems of plasma physics. The key physics in our case is capillary-driven creeping flow within the roughness-defined channels, which are connected at the grain contacts by the liquid bridges. Our model can be easily scaled down or up as needed to describe transport in fine nanoparticle assemblies or in coarse granular materials.

Acknowledgment. This work is supported by the Joint Science and Technology Office, Defense Threat Reduction Agency (JSTO/DTRA), Threat Agent Science (TAS) of the US Department of Defense.

---

[1] M Scheel et al. (2008) Nature Materials 7 189–193.
[2] M Scheel et al. (2008) J. Phys. Condens. Matter 20 494236.
[3] S. Herminghaus (2005) Advances in Physics 54 221-261.
[4] Bear, J. *Dynamics of Fluids in Porous Media*, Dover Publications Inc. NY. (1972).
[5] Orr, F.M., Scriven, L.E., Rivas, A.P., (1975) J. Fluid Mech. 67 723–742.
[6] Rye, R.R., Yost, F.G., O$'$Toole, E.J., (1998) Langmuir 14 3937–3943.
[7] Bico, J., Thiele, U., Quere, D., (2002) Colloid Surface A 206 41-46.
[8] Whitaker, S., (1969) Ind. Eng. Chem. 61 14-28.
[9] J.L. Vazquez, *The porous medium equation - Mathematical theory* Oxford Mathematical Monographs (2006)
[10] M.J.Baines, M.E.Hubbard, P.K.Jimack, (2011) Comm. Comput. Phys. 10 509–576..
[11] Alshibli, K.A., Alsaleh, M.I., (2004) J. Comput. Civil Eng. 18 36–45.
[12] The Center for Research Information, Inc., 9300 Brookville Rd, Silver Spring, MD 20910, *Health Effects of Trioctyl Phosphate* Contract No. IOM-2794-04-001 of the National Academies (2004).

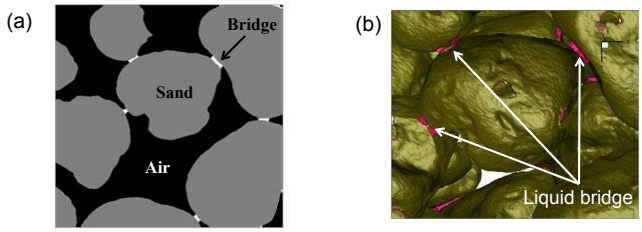

Figure 1: Illustration of isolated bridges at low levels of saturations. (a) MicroXCT image, typical from our experiments. (b) 3D image reconstruction of MicroXCT data. The liquid within the roughness of the sand grains, as discussed further below, is invisible to MicroXCT.

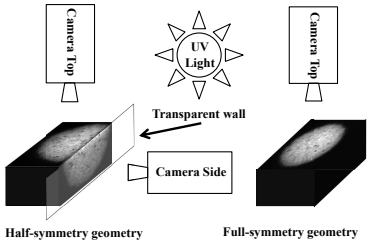

Figure 2: Illustration of the experimental setup in the full and in the half-symmetry geometries.

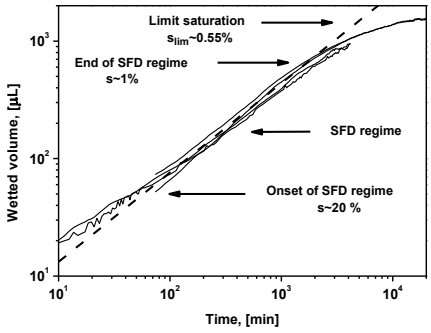

Figure 3: Spreading of $2.8\,\mu$L TEHP liquid drops in sand in full symmetry: 4 different tests. The dashed line shows power law $V(t) \sim t^{0.75}$. The data points are so close in time that they merge into continuous lines.

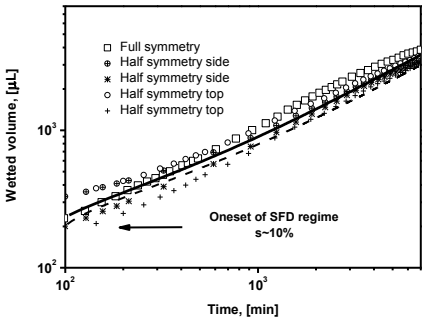

Figure 4: Spreading of $6\,\mu$L drops of TEHP in sand. Full and half-symmetry geometries. Many in-between data points were deleted for clarity of presentation. The solid and the dashed lines are numerical solutions to (5) for $6\,\mu$L and $12\,\mu$L drops respectively, which are roughly the power law $V(t) \sim t^{0.67}$. The wet volume in the $12\,\mu$L simulation is halved to mimic the half-symmetry case.